

Article

Implementation of Modified Compression Field Theory to Simulate the Behavior of Fiber-Reinforced Polymer Shear-Strengthened Reinforced Concrete Beams under Monotonic Loading

Nagwa Ibrahim ¹, Said Elkholy ², Ahmed Godat ^{3,*} and Ahmed El-Kholy ²

¹ Department of Civil and Environmental Engineering, United Arab Emirates University, Al-Ain P.O. Box 155551, United Arab Emirates

² Department of Civil Engineering, Fayoum University, Fayoum 2933110, Egypt

³ Department of Civil Engineering, Ajman University, Ajman P.O. Box 346, United Arab Emirates

* Correspondence: a.godat@ajman.ac.ae

Abstract: The numerical modeling of structures is a widely preferable approach to investigate the structural behavior of RC beams since it delivers inexpensive predictions for confirming the required goals concurrently with reducing casting, testing time, and effort. Shear-strengthening of reinforced concrete (RC) beams using externally bonded (EB) fiber-reinforced polymers (FRPs) has attracted much attention due to the fact that the FRP strengthening technique has the ability to alter the distribution of stresses between the structural elements and increase the load-carrying capacity. A significant number of experimental studies have been carried out to test the monotonic behavior of FRP shear-strengthened RC beams. Conversely, limited numerical research has been performed to investigate such performance. The VecTor2 software is developed based on the modified compression field theory (MCFT) and is directed to examine the monotonic behavior of retrofitted specimens using fiber-reinforced polymer (FRP) composites. To the authors' knowledge, the behavior of FRP shear-strengthened beams has not been explored in the literature using the MCFT modeling approach. The main objective of this study is to detect the software's capability of predicting the experimental outcomes of FRP shear-strengthened RC beams. This research study is carried out in two stages. Initially, the numerical study involves the development of an accurate finite element model to simulate the control specimens. The quality of this model is assessed by comparing the numerical results with the experimental outcomes. In the second phase of the numerical study, the control beam model is modified to accommodate the presence of external FRP composites. The accuracy of this model is again measured by comparing its predictions with the experimental measurements. The goal of these phases is to ensure that the numerical model captures the actual behavior of the tested beams. Additionally, two distinctive modeling approaches are investigated to represent the behavior of FRP composites. The accuracy of the numerical models is verified through comparisons of numerical predictions to experimental results in terms of ultimate loading capacity, load–deflection relationships, and failure modes. It can be stated that the validated numerical model provides alternate means for evaluating the monotonic behavior of both strengthened and non-strengthened RC beams. The predicted results compare very well with the test results of the control specimens when discrete truss elements are employed for the FRP composites. Furthermore, the numerical model provides useful information on the crack patterns and failure modes.

Keywords: finite element simulation; VecTor2 software; reinforced concrete beams; fiber-reinforced polymers; monotonic loading; shear strengthening; load–deflection response; smeared layer element; discrete truss element; failure mode



Citation: Ibrahim, N.; Elkholy, S.; Godat, A.; El-Kholy, A.

Implementation of Modified Compression Field Theory to Simulate the Behavior of Fiber-Reinforced Polymer Shear-Strengthened Reinforced Concrete Beams under Monotonic Loading. *Buildings* **2023**, *13*, 898. <https://doi.org/10.3390/buildings13040898>

Academic Editors: Chiara Bedon and Savvas Triantafyllou

Received: 2 February 2023

Revised: 26 February 2023

Accepted: 13 March 2023

Published: 29 March 2023



Copyright: © 2023 by the authors. Licensee MDPI, Basel, Switzerland. This article is an open access article distributed under the terms and conditions of the Creative Commons Attribution (CC BY) license (<https://creativecommons.org/licenses/by/4.0/>).

1. Introduction

An extensive number of existing reinforced concrete structures are persistently exposed to damage induced by the deterioration of concrete, natural environmental effects, and corrosion of steel. This might be attributed to the continuous increase in the load requirements compared to what they were originally designed for, the change in the structure's function, and the necessity to meet the current design standards [1]. Repair and strengthening would be an efficient or economical option instead of removing all these structures and replacing them with new ones [2,3]. As a contribution to filling this demand, significant attention has been directed toward strengthening RC structures and restoring their capacity as a viable and cost-effective method.

Among the available potential methods of structures rehabilitation and strengthening techniques, external strengthening by the utilization of fiber-reinforced polymer composites has gained vast popularity and massive acceptance by practical engineers [4] for their leading potentials, such as limiting and controlling the cracks, improving the load-carrying capacity, increasing stiffness with an effective cost exceeding those of conventional steel [5,6].

The shear strength of RC structures is usually affected by the existence of cracks, loading history, and the heterogeneity of the concrete [7]. Shear failure of reinforced concrete (RC) beams is known to be brittle. This occurs without prior sufficient warnings, which in turn results in serious damages [8]. Therefore, the need for shear strengthening is crucial and requires appropriate attention to hinder such catastrophic failure. The shear failure of either strengthened or un-strengthened RC beams is usually initiated through a critical major diagonal crack that starts with a flexural crack at the beam's soffit, followed by crack propagation rising to the top surface of the beam [9,10]. This mode of failure is normally undesirable compared to the flexural mode of failure because the latter is ductile, which makes it preferable [10]. This can be accomplished by increasing the shear strength and activating the flexural mode of failure as the controlling one, hence providing ductile behavior [11]. FRP shear-strengthening of RC beams is significantly required where they are deficient in shear or if their shear capacity is less than their flexural capacity [8]. Accordingly, a formidable number of experimental studies available in the literature have been carried out on statically loaded FRP shear-strengthened beams and investigated their feasibility. These studies have concluded and proved the applicability of improving (repairing and upgrading) the shear strength of RC members employed by externally affixing the FRP composites perpendicular to both the member and the expected shear cracks' locations.

Non-linear finite element analysis (NLFEA) computer software simulation of reinforced concrete (RC) structural elements has attracted immense attention during the last few decades due to their distinguished power to follow identical patterns of very complicated real-life behavior [12]. It showed great capability in considering the complicated elements' geometries, loading nature, and the complexity of the material's constitutive relationships, which failed to be considered in the traditional design equations [13]. However, to the best of the authors' knowledge, bounded numerical studies have particularly addressed the monotonic behavior of FRP shear-strengthened beams [14]. One of these numerical studies was carried out by Chen et al. [15,16] to examine the effect of the bond–slip relationship by utilizing various material interfaces on the behavior of the FRP shear-strengthened RC beams. These interfaces were whether between the concrete and internal reinforcement (longitudinal and transverse) or between the external FRP and the concrete substrate. The numerical investigation was implemented using ABAQUS software. Initially, it has been validated against several studies in terms of load–deflection response, failure modes, FRP strains, and crack patterns. The validated finite element model was extended afterward to examine the influence of various bond–slip (concrete-to-reinforcement and concrete-to-FRP) models on the shear behavior. The finite element model showed good agreement with the experimental results regarding the crack pattern and the failure modes. For the same experimental set, the control specimen failed in shear tension, whereas the strengthened specimen failed in FRP debonding. The study emphasized the importance of adopting

appropriate models regarding the concrete/longitudinal steel, concrete/transverse steel, and concrete/FRP interfaces due to their serious effect on the performance of FRP shear-strengthened RC beams and the accuracy of the numerical simulation.

Arduini et al. [17] carried out experimental and numerical programs on a two-span beam to study the performance of RC beams strengthened with FRP sheets. A perfect bond was assumed between the FRP and the concrete. Despite that the numerical predictions of Arduini et al. roughly overestimated the peak loads and midspan deflections in addition to a less ductile load–deflection response, the overall numerical estimations were compatible with the experimental measurements.

An analytical model was developed by Malek and Saadatmanesh [18,19] through the utilization of ABAQUS software, where a perfect bond was assumed between the FRP and the concrete. The two-dimensional model resulted in a relative overestimation in the resulted strains of the FRP even though they were in good agreement with the experimental results.

In the numerical study of Kachlakev and McCurry [20] using ANSYS finite element software, the specimens were shear-strengthened by externally attaching the FRP laminated on the concrete elements assuming a perfect bond. Although the experimental and the numerical outcomes were well-matched, the midspan deflections and the peak loads were insignificantly overestimated. Al-Mahaidi et al. generated a finite element model using DIANA software to examine the behavior of FRP shear-strengthened beams. The numerical predictions revealed that the tensile strain in the FRP composites was less than the experimental results. Moreover, the estimated load-carrying capacities were inferior to the experimental counterparts.

A numerical study was performed by Wong et al. [21] to examine the response of FRP shear-strengthened beams using an in-house finite element model. The bond–slip response between the concrete and the FRP was adopted by including two distinctive bonding relationships: (i) linear–elastic and (ii) linear–plastic. It was concluded that the numerical predictions obtained using the latter were more reliable and accurate. A premature failure was obtained due to the implementation of the second FRP to concrete relationship.

This research paper ultimately aims to create a valid, viable, and robust two-dimensional finite element model that has the potential to simulate the performance of both un-strengthened and FRP shear-strengthened (RC) beams when subjected to monotonic loading using the VecTor2 software. Its modeling library includes an enormous variety of models to represent the concrete's strengths, post-peak behavior, failure modes, crack patterns, deflections, etc. Furthermore, the software is characterized by its potential to represent the member's diverse material properties, their complicated geometries, and the type of loading. The software has the potential to perform the analysis under different types of loads positioned into three categories: monotonic, cyclic, and reverse cyclic loadings [12,13]. Eventually, once the accuracy of the developed finite element (FE) models is confirmed, they can be utilized for achieving the following objectives:

1. Improve understanding of the VecTor2 software to model the behavior of control specimens under monotonic loading;
2. Simulate the behavior of FRP shear-strengthened RC beams subjected to monotonic loading using the VecTor2 software;
3. Compare the effectiveness of two methodologies to model the FRP composites for shear strengthening to select the method that captures the actual response.

2. Modified Compression Field Theory (MCFT)

VecTor2 software is a computer program for two-dimensional non-linear finite element analysis (NLFEA) of reinforced concrete members. The concrete model of this software was established on the basis of MCFT. The theory was developed by Vecchio and Collins [22] and approved by the ASSHTO and CSA design codes [23]. They have carried out an experimental program to examine the behavior of reinforced concrete panels subjected to biaxial stresses (combined normal and shear stresses) along with pure shear. An analytical model for cracked concrete was proposed by considering a new material with different

stress–strain properties. In addition, they anticipated a pattern for the load–deflection relationship of RC elements subjected to in-plane normal and shear stresses [12,13,22]. In the MCFT theory, the cracked concrete is treated as an orthotropic material, and the smeared rotating crack approach is implemented to achieve compatible crack patterns with those detected in many RC members [24–26]. Additionally, the smeared rotating cracks are automatically redirected without any restraint to be aligned with the direction of the principal concrete compressive stress field [12,27]. Furthermore, the MCFT relies on several major assumptions [12,28]:

1. The smeared rotating cracks are uniformly distributed;
2. The reinforcements are uniformly distributed;
3. Full contact bond between the concrete and the reinforcing steel;
4. The cumulative strain history is neglected, and each strain phase is independent of the precedent;
5. The three sets creating the MCFT are expressed in the form of average stresses and strains;
6. At crack locations, local strains and stresses are accounted for.

The MCFT concrete model considers the features of compatibility, equilibrium, and constitutive relationships. In addition, the model employs failure envelopes to define failure in either tension or compression. It also adopts a mechanism to model the post-cracking and post-crushing behavior of the concrete.

Compatibility, Equilibrium, and Constitutive Relationships

Regarding the compatibility relations, the MCFT considers the average strain of the concrete and steel, as depicted in Figure 1.

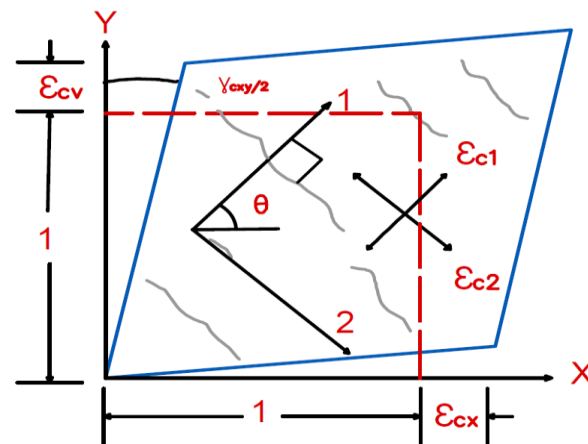


Figure 1. Average Concrete Strains [12,29].

The MCFT assumes a perfect bond between the concrete and the reinforcing steel. The average strains experienced by both the concrete and the reinforcing steel are expected to be identical. Accordingly, the compatibility equations are expressed as follows [12,28]:

$$\varepsilon_x = \varepsilon_{cx} = \varepsilon_{sx} \quad (1)$$

$$\varepsilon_y = \varepsilon_{cy} = \varepsilon_{sy} \quad (2)$$

where ε_x and ε_y indicate the total strain in the x and y directions, respectively; ε_{cx} and ε_{cy} denote the average concrete strain in the x and y directions, respectively; and ε_{sx} and ε_{sy} represent the average steel strain parallel to the x and y directions, respectively. The free-body diagram for the average stresses in the concrete and the reinforcing steel ($f_{cx}, f_{cy}, f_{sx}, f_{sy}$) is presented in Figure 2.

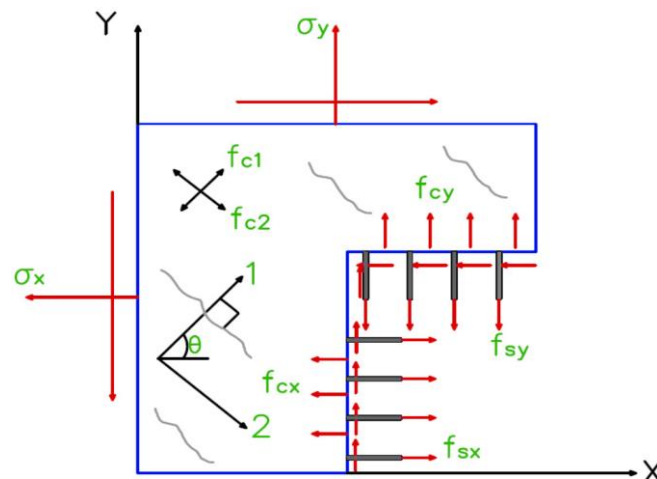


Figure 2. Free-Body Diagram of the Average Stresses in Reinforced Concrete [12,29].

The applied stresses (σ_x, σ_y) should be in balance with the applied stresses for the concrete and reinforcing steel [12,28]. Thus, the equilibrium equations can be expressed in the following forms:

$$\sigma_x = f_{cx} + \rho_{sx}f_{sx} \quad (3)$$

$$\sigma_y = f_{cy} + \rho_{sy}f_{sy} \quad (4)$$

where σ_x and σ_y are the applied stress in the x and y directions, respectively; f_{cx} and f_{cy} are the average concrete stress parallel to the x and y directions, respectively; f_{sx} and f_{sy} represent the reinforcement stresses in the x and y directions, respectively; and ρ_{sx} and ρ_{sy} are the reinforcement ratios in the x and y directions, respectively.

The compatibility equations (strains) and the equilibrium conditions (stresses) are linked to formulate the constitutive models, particularly for cracked concrete under compression and tension. The principal compressive stress f_{c2} is related to the principal compressive strain ε_{c2} in terms of concrete in compression. The compression softening phenomenon is detected through experimental tests. Whenever the compressive strength and the stiffness decrease, the principal tensile strain increases based on the following expression [12]:

$$f_{c2} = \frac{f'_c \left[2 \left(\frac{\varepsilon_{c2}}{\varepsilon_0} \right) - \left(\frac{\varepsilon_{c2}}{\varepsilon_0} \right)^2 \right]}{0.8 - 0.34 \left(\frac{\varepsilon_{c1}}{\varepsilon_0} \right)} \quad (5)$$

where f_{c2} represents the concrete principal compressive strength; ε_{c2} indicates the corresponding concrete principal compressive strain; ε_0 is the concrete cylindrical strain, which corresponds to its peak compressive stress usually designated as f'_c ; and ε_{c1} refers to the concrete tensile strain. It may be worth noting that the denominator in Equation (5) exemplifies the softening phenomenon of the principal tensile strain. As for the concrete in tension, the principal tensile stress f_{c1} is correlated with the principal tensile strain ε_{c1} . The cracking tensile strength f'_t must be initially computed as well as the cracking strain ε_{cr} as follows:

$$f'_t = 0.33 \sqrt{f'_c} \quad (6)$$

$$\varepsilon_{cr} = \frac{f'_t}{E_c} \quad (7)$$

where the concrete initial tangent stiffness E_c is computed in accordance with the following equation:

$$E_c = 5000 \sqrt{f'_c} \quad (8)$$

3. Finite Element Modeling

The VecTor2 software applied the constitutive relationships of the MCFT. Thereafter, its power has been expanded to closely resemble the cracked concrete by means of encountering second-order material models such as compression softening, tension softening, tension stiffening, etc. [12,23,26]. The VecTor2 adequately models reinforced concrete structures as it employs a fine mesh of low-powered elements, which fulfills the need to simulate the crack patterns with high numerical stability [12,23,26,28]. In this section, the properties of the computer software to simulate the behavior of concrete, reinforcing steel, and FRP composites are provided.

3.1. Material Modeling

Concerning the constitutive laws, the VecTor2 software library contains numerous options to represent the behavior of concrete, steel, and FRP reinforcements. Table 1 lists the appropriate models that are selected to accurately simulate the response of the control as well as the FRP shear-strengthened RC beams.

Table 1. Materials Models for Concrete, Reinforcing Steel, and FRP [30,31].

Material	Factor	Constitutive Model
Concrete	Compression Pre-Peak	Hognestad (Parabola)
	Compression Post-Peak	Modified Park–Kent
	Compression Softening	Vecchio 1992-A (e1/e2-Form)
	Tension Stiffening	Modified Bentz 2005
	Tension Softening	Non-Linear (Hordjik)
	Confined Strength	Kupfer/Richart
	Cracking Criterion	Mohr–Coulomb
Steel Reinforcement	Reinforcement Stress–Strain	Elastic–Plastic
FRP	FRP Stress–Strain	Linear Elastic

3.1.1. Concrete

The ascending branch of the concrete stress–strain response (compression pre-peak) is modeled using the Hognestad (Parabola) model. This model is adopted according to the comparison between numerical predictions and experimental results for various pre-peak models available in the software, as shown in Figure 3a. Hognestad (Parabola) model is preferred because it provided better numerical predictions in terms of peak load compared to the experimental results. The Hognestad (Parabola) model is characterized by linear behavior until reaching approximately 70% of the concrete compressive strength. Afterward, the stress–strain relationship converts to non-linear behavior up to failure [32–34], as depicted in Figure 3b.

For the descending branch of the stress–strain concrete curve (compression post-peak), the widely used “Modified Park–Kent” model was implemented based on the comparison shown in Figure 4a between the models available in the software. In Figure 4b, f'_c and ε_o refer to the concrete compressive strength and the corresponding concrete compressive strain, respectively. Additionally, $0.2f'_c$ and ε_{c20} represent 20% of the concrete compressive strength and the corresponding compressive strain, respectively. In the “Modified Park–Kent” model, a gradual linear decrease in the concrete strength is observed to a value of about 20% of its peak. Additionally, the model considers the confinement effect to enhance the concrete ductility and strength.

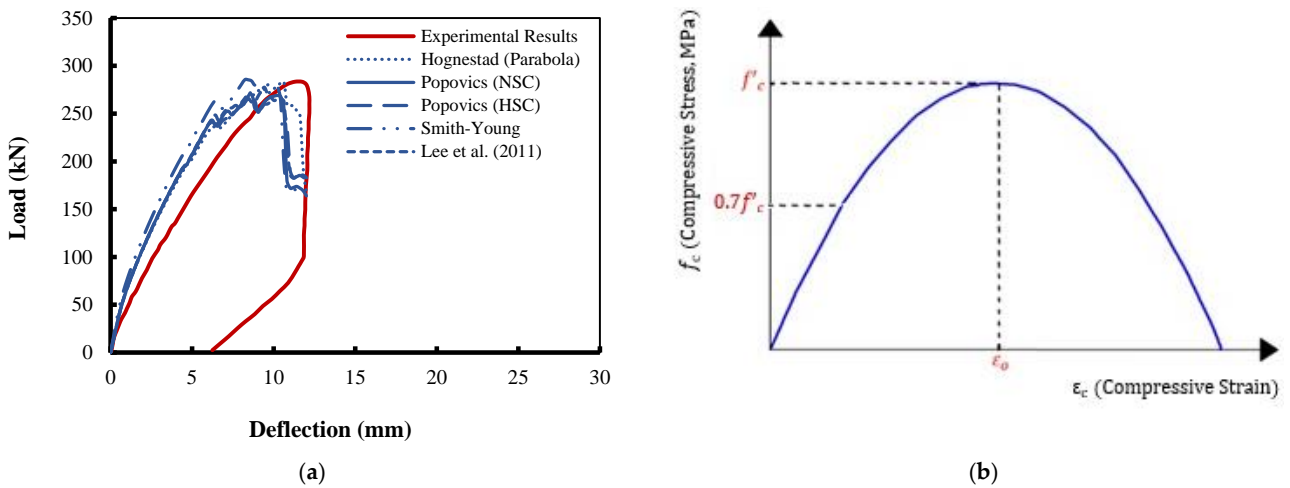


Figure 3. Concrete Compression Pre-Peak Response: (a) Comparison between Concrete Compression Pre-Peak Models Available in VecTor2; (b) Concrete Hognestad (Parabola) Pre-Peak Model [32,33].

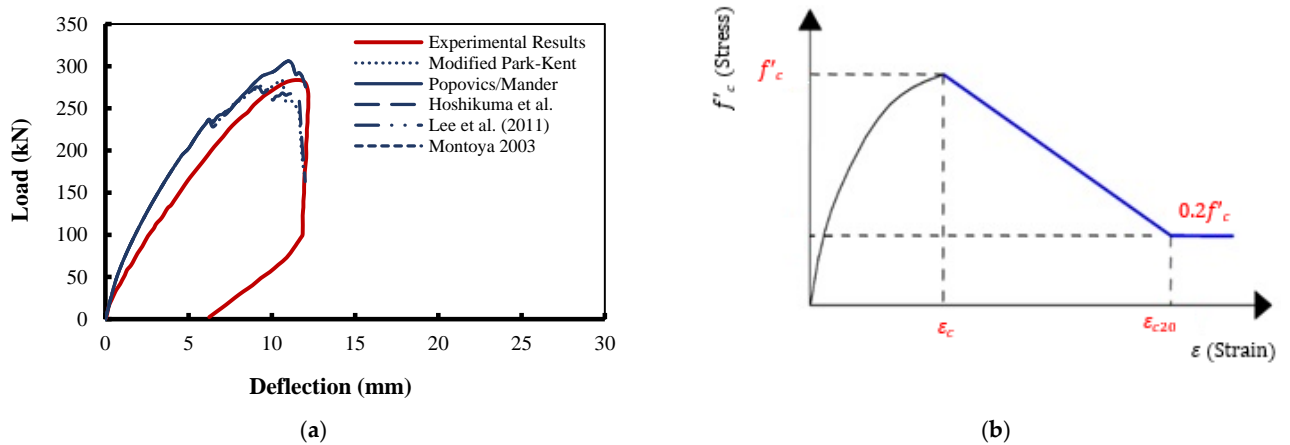


Figure 4. Concrete Compression Post-Peak Response: (a) Comparison between Concrete Compression Post-Peak Models Available in VecTor2; (b) Concrete Modified Park-Kent Pre-Peak Model [32,35].

In tension, the concrete behaves as linear elastic up to the point where cracking is initiated, as shown in Figure 5. The tension stiffening, which occurs beyond the ultimate tensile strength, is simulated by employing the Modified Bantz model [24,35–37]. The tension stiffening is a significantly required feature to capture the load–deformation relationship. Generally, the compressive strength, f'_c , is extracted from the experimental data.

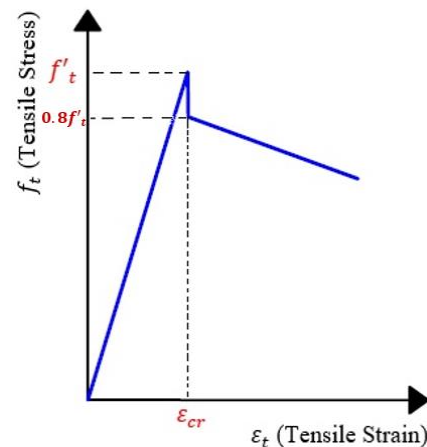


Figure 5. Concrete Tensile Stress–Strain Curve [38].

3.1.2. Steel Reinforcement

The steel reinforcement has identical elastic–plastic behavior in tension and compression, as depicted in Figure 6. It initiates with a linear response that terminates at the yielding stress, followed by a yielding plateau. The strain hardening can be modeled as linear or non-linear behavior based on the type of steel, whereas the effect of non-linear strain hardening is excluded by the ACI guideline; hence, a linear stage has been proposed for the strain hardening [23,39].

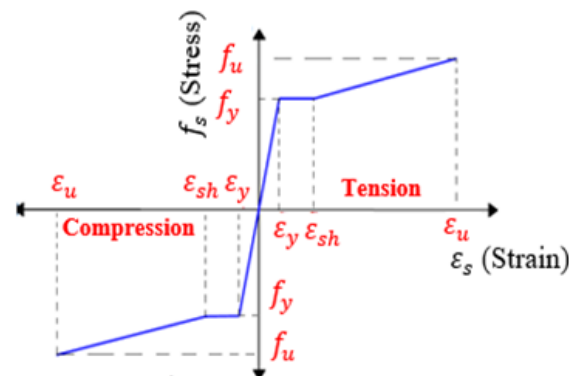


Figure 6. Steel Stress–Strain Curve [40,41].

3.1.3. Fiber-Reinforced Polymers

The behavior of the FRP materials is taken as a linear elastic material, where it usually behaves elastically linear until the rupture point with the absence of any yielding stage [14,23,39,42–45], as shown in Figure 7.

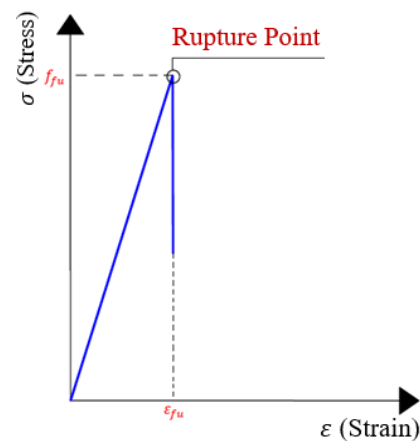


Figure 7. Fiber-Reinforced Polymer Stress–Strain Curve [39].

3.2. Structural Modeling (Concrete and Reinforcement Elements)

The VecTor2 software provides three element types, which are constant strain triangle elements (CST), plane stress rectangle elements, and quadrilateral elements. In this study, the concrete elements are modeled using four-node plane stress rectangular elements with eight degrees of freedom (two degrees of freedom per node). The structural steel plates, which are placed on the locations of the applied loads and the support points, are modeled likewise. For the steel reinforcements, whether longitudinal or transverse, two-node discrete truss elements of two degrees of freedom at each node are adopted. The steel reinforcement is assumed to be perfectly bonded to the concrete elements, as this has been proven to be reliable and workable in many studies [46].

The VecTor2 software provides two possible options to model the FRP composites: (1) discrete truss elements and (2) smeared layer elements [47]. The latter method focuses on simulating the FRP composites as continuous FRP sheets with fibers aligned vertically (90°

from the x -axis). The former method functions by converting the FRP into equivalent truss elements with a specific diameter and cross-sectional area. Considerable numerical models investigated the modeling of FRP composites using one of the previous methods, whereas few investigations verified both methods simultaneously [23,28,45]. To the best of the authors' knowledge, there is no published numerical study investigating the two methods to model the FRP composites for shear strengthening response of RC beams using the VecTor2 software. In this study, both methods of simulating the FRP composites are carried out; hence, each FRP shear-strengthened specimen is modeled twice: once with a smeared layer element and once with a discrete truss element. This is followed by comparing the two modeling methods to eventually recommend the best one that can be utilized to accurately model the FRP composites.

Regarding the concrete-to-FRP bond, debonding of FRP composites from the concrete substrates is usually of vital importance and major concern. The actual bond behavior between the FRP composites and the concrete should be taken into account to attain an inclusive and thorough finite element model. However, no debonding failure was observed in the tested beams considered for the current finite element model verification. Therefore, a perfect bond between the FRP composites and the concrete is assumed.

3.3. Sensitivity Analysis

To study the effect of the meshing size on the accuracy of the developed FE models, different mesh sizes are attempted to specify the sufficient mesh size. It should be mentioned that a mesh sensitivity analysis is carried out for each control specimen to specify the appropriate mesh size. For instance, a square mesh size of 25×25 mm for Murthy et al. [48] showed load–deflection behavior similar to the experimental one, as illustrated in Figure 8. Furthermore, the maximum loading capacity of this mesh size is comparable to the experimental one.

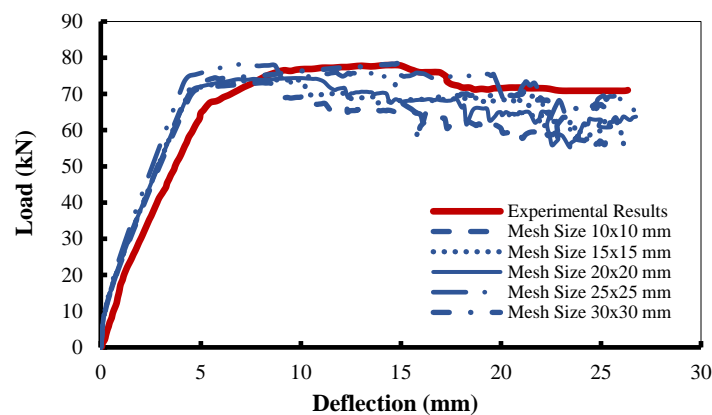


Figure 8. Sample of Mesh Sensitivity Analysis (Murthy et al. [48]).

3.4. Modelled Test Specimens

In this study, a total number of eleven tested specimens from the available literature are extracted, modeled, and addressed. A full description of the adopted specimens regarding their geometry, designation, and loading conditions is provided in Table 2, whereas Tables 3 and 4 illustrate their material properties.

The first set of numerically simulated specimens was experimentally tested by Murthy et al. [48]. The control specimen of this study labeled as “CBA” had 35 MPa concrete compressive strength and rectangular cross-section (200×100 mm), as illustrated in Figure 9. The beam was tested under four-point bending spanned over 1200 mm. For the longitudinal reinforcement, two bars of 10 mm and another two of 8 mm were placed at the bottom and top of the beams, respectively.

Table 2. Specimens Geometrical Characteristics.

Number	Specimen	Beam Dimensions (mm)					a/d ⁶	Cross-Section	Beam Status
		L ¹	b_w ²	b_f ³	h_w ⁴	h_f ⁵			
1 [48]	CBA	1200	100	-	200	-	2.00	R-Beam	Control
2 [49]	C	1500	150	-	200	-	2.50	R-Beam	Control
3 [50,51]	N-1	1220	152.4	-	152.4	-	2.67	R-Beam	Control
4 [7]	FB30-1	1500	150	-	300	-	1.67	R-Beam	Control
5 [7]	FB30-2								Strengthened
6 [7]	FB30-3								Strengthened
7 [52,53]	CON-S0	3110	152	508	304	102	3.00	T-Beam	Control
8 [52,53]	CON-S1								Control
9 [52,53]	CON-S3								Control
10 [2,54–56]	S1-0.33R								Strengthened
11 [2,54–56]	S3-EB								Strengthened

¹ Span length; ² web width; ³ flange width; ⁴ web height; ⁵ flange height; ⁶ shear span-to-depth ratio.

Table 3. Specimens Material Properties.

Number	Specimen	f'_c ¹ (MPa)	Longitudinal Steel				Transverse Steel	
			Top		Bottom		Dia. (mm) at Spacing (mm)	Yield Stress (MPa)
			Dia. ² (mm)	Yield Stress (MPa)	Dia. (mm)	Yield Stress (MPa)		
1 [48]	CBA	35	2 Ø 8	300	2 Ø 10	590	Ø 6 @ 100	240
2 [49]	C	35	2 Ø 8	300	3 Ø 12	420	Ø 8 @ 120	300
3 [50,51]	N-1	39.3	2 Ø 13	427	2 Ø 13	427	Ø 10 @ 50	320
4 [7]	FB30-1	25	2 Ø 8	330	2 Ø 14	410	Ø 6 @ 150	240
5 [7]	FB30-2							
6 [7]	FB30-3							
7 [52,53]	CON-S0	31	6 Ø 10	480	2 Ø 25	500	None	-
8 [52,53]	CON-S1						Ø 8 @ 175	540
9 [52,53]	CON-S3						Ø 8 @ 260	540
10 [2,54–56]	S1-0.33R						Ø 8 @ 175	540
11 [2,54–56]	S3-EB						Ø 8 @ 260	540

¹ Concrete compressive strength; ² bar diameter.

Table 4. Mechanical Properties of FRP Materials.

Number	Specimen	FRP Type	t_f ¹ (mm)	w_f ² (mm) at Spacing	Ultimate Strength (MPa)	E ³ (GPa)	Ultimate Strain (%)
5 [7]	FB30-2	CFRP Strips	0.11	50 @ 50	4103	242	1.7
6 [7]	FB30-3	GFRP Strips	0.27	50 @ 50	3400	73	2.7
10 [2,54–56]	S1-0.33R	CFRP Sheet	0.11	-	3450	230	1.33
11 [2,54–56]	S3-EB	CFRP Sheet	0.11	-	3450	230	1.33

¹ FRP thickness; ² FRP strip width; ³ FRP modulus of elasticity.

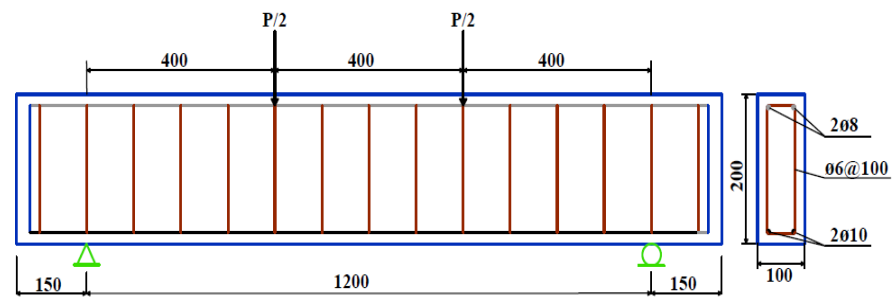


Figure 9. Detailed Geometry of Murthy et al. Specimen (CBA) [48].

Another set of experimental programs that were tested under four-point bending by Banjara and Ramanjaneyulu [49] is investigated in this study. The control beam designated as “C” is modeled. The concrete compressive strength of the specimen was 35 MPa, and it was made of a rectangular cross-section (200×150 mm), as shown in Figure 10. The flexural reinforcement of the specimen is composed of three steel bars of 12 mm in the beam’s tension zone and two 8 mm bars in the compression zone. Transverse steel of 8 mm was spaced at intervals of 120 mm.

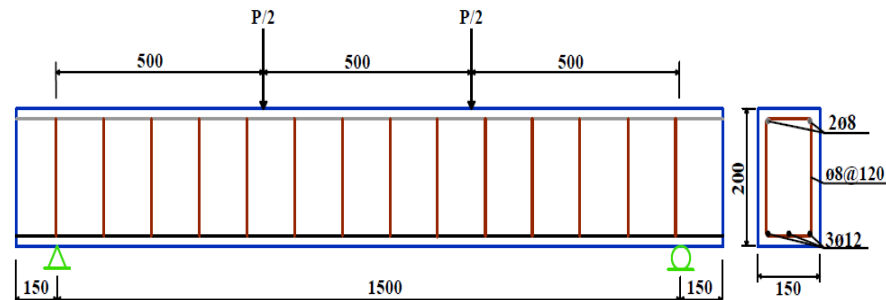


Figure 10. Detailed Geometry of Banjara and Ramanjaneyulu Specimen (C) [49].

As a means of further exploration of the monotonic behavior of RC beams, the control specimen labeled as “N-1” of the experimental study carried out by Papakonstantinou [50,51] is considered. The RC beam had a concrete compressive strength of 40 MPa and a rectangular cross-section of 152.4×152.4 mm in a span length of 1220 mm and was tested under monotonic loading, as shown in Figure 11. The beam was reinforced with two bars of 13 mm located at both the compression and tensile zones. The internal steel stirrups were 10 mm in diameter and spaced at 50 mm intervals.

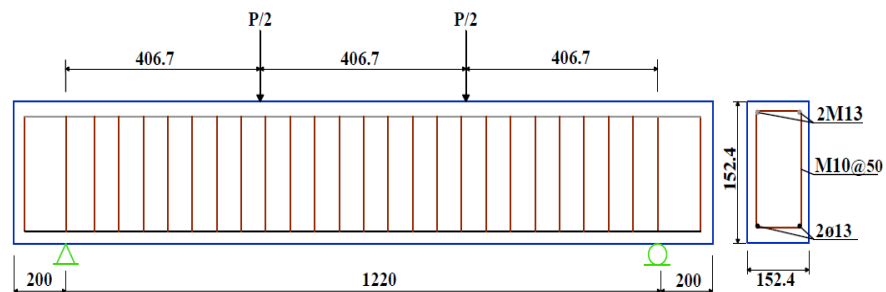


Figure 11. Detailed Geometry of Papakonstantinou et al. Specimens (N-1) [50,51].

An extra set of experimentally investigated specimens by Dong et al. [7] and having a concrete compressive strength of 25 MPa are considered in the current study. These specimens had a rectangular cross-section (300×150 mm) over an effective span of 1500 mm and were tested under four-point bending, as depicted in Figure 12. Furthermore, these beams were reinforced with two bars of 8 mm in the compression zone and two bars of 14 mm in the tension zone. Steel stirrups of 6 mm were placed at every 100 mm interval.

Additionally, a control specimen labeled as “FB30-1” and two FRP shear-strengthened specimens labeled as “FB30-2” and “FB30-3” are numerically simulated in this study. The shear strengthening was externally applied in a U-wrap arrangement as FRP sheet strips for “FB30-2” and “FB30-3” specimens, respectively, as provided in Figure 13.

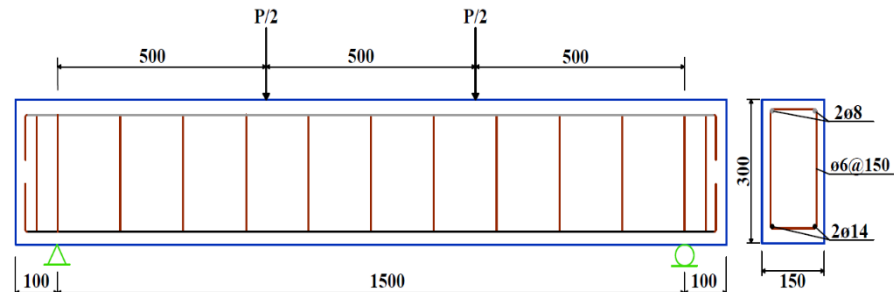


Figure 12. Detailed Geometry of Dong et al. Control Specimen (FB30-1) [7].

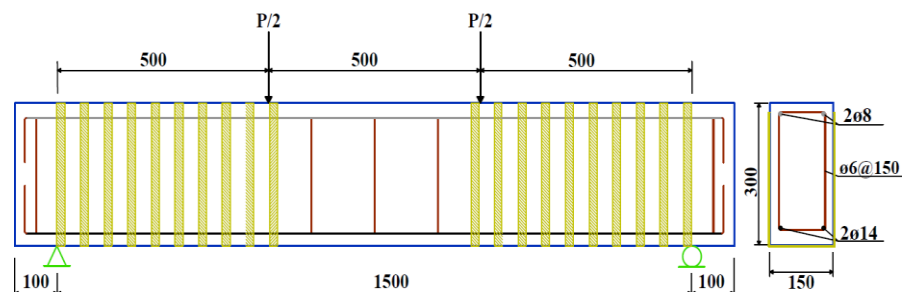


Figure 13. Detailed Geometry of Dong et al. CFRP-Strengthened Specimens (FB30-2 and FB30-3) [7].

To further evaluate the reliability of the non-linear FE models, an additional set of experimental tests conducted by Chaallal et al. [52–56] is considered. The experimental programs consisted of three groups of specimens with three control ones. All the beams typically comprised a T-cross-section (508×102 mm for the flange and 304×152 mm for the web) with an effective span length of 3110 mm, as presented in Figure 14. The unique aspect that distinguishes these three control specimens is the existence of steel stirrups, where the “CON-S0” specimen was free of steel stirrups, while the other two specimens contained steel stirrups spaced at 175 mm and 260 mm and were labeled as “CON-S1” and “CON-S3”, respectively. The longitudinal steel reinforcement at the bottom of the beam was of four bars of 25 mm located in two layers. However, six bars of 10 mm were positioned at the top of the cross-section. The three control specimens are numerically analyzed in this research paper. The research study of Chaallal et al. involved two FRP shear-strengthened with continuous sheets along the shear span designated as “S1-0.33R” and “S3-EB” [2,54–56], as shown in Figure 15. The two specimens were tested under monotonic loading. Note that all mentioned parameters of Table 2 are shown in Figure 16.

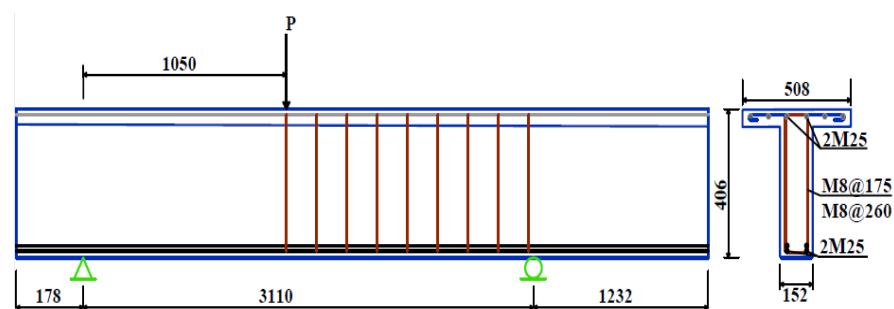


Figure 14. Detailed Geometry of Chaallal et al. Control Specimens (CON-S0, CON-S1, CON-S3) [52,53].

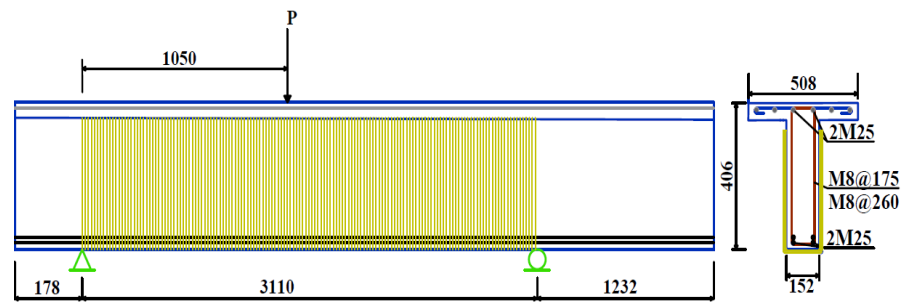


Figure 15. Detailed Geometry of Chaallal et al. CFRP-Strengthened Specimens (S1-0.33R, S3-EB) [54–56].

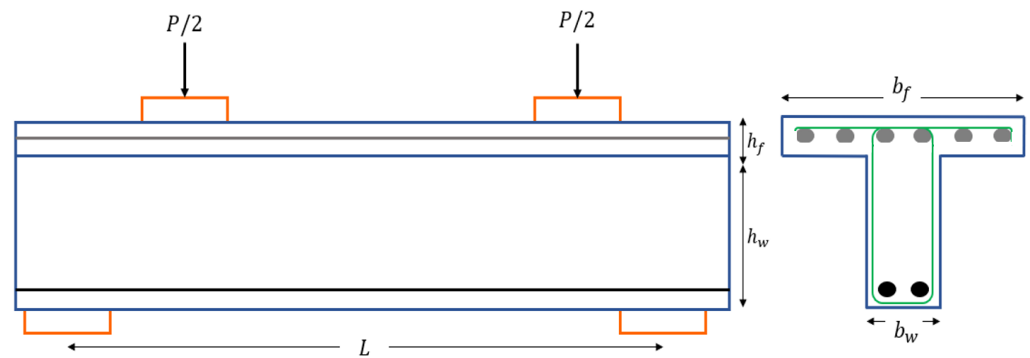


Figure 16. Typical Geometrical Characteristics of a T-Beam.

Various numerical models are generated under monotonic loading and validated against the experimental results to evaluate their reliability in predicting the monotonic behavior of both control and FRP shear-strengthened specimens. Figure 17 demonstrates a typical beam model of the present study.

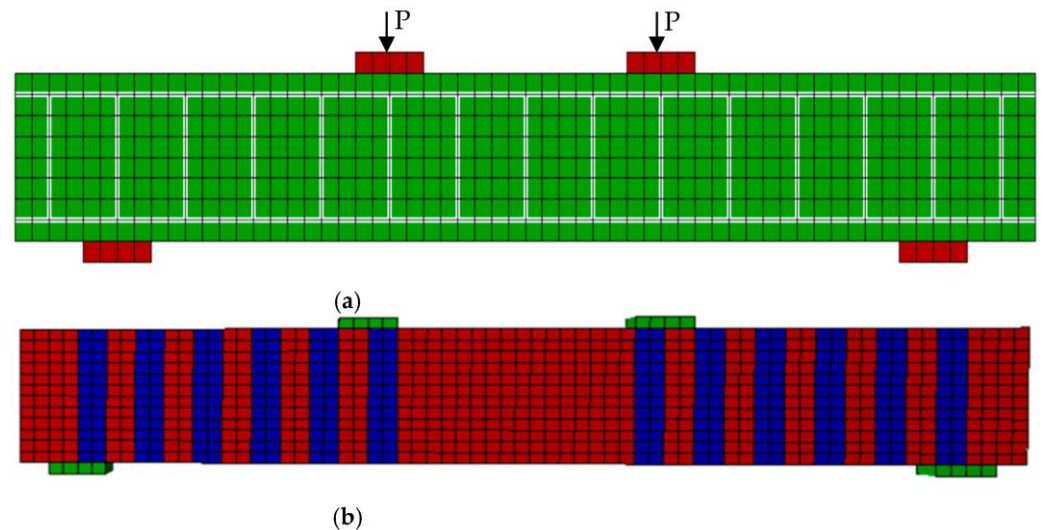


Figure 17. Typical Two-Dimensional View of the Generated Finite Element Models: (a) Typical Control Specimen; (b) Typical Specimen Strengthened with FRP Strips.

4. Results and Discussions

The results presented in the subsequent sections are in terms of ultimate load carrying capacity " $P_{ult,exp}$ " and the corresponding deflection " $\delta_{ult,exp}$ " in addition to the load at failure " $P_{f,exp}$ " and the corresponding deflection at failure " $\delta_{f,exp}$ ". The numerical predictions are compared to experimental results for the different simulated specimens. Note that the ultimate load-carrying capacity corresponds to the peak loading value.

4.1. Validation of Control Specimens

The fundamental stage of the present study is to verify the accuracy of the proposed non-linear finite element models against a series of control specimens that were experimentally tested under monotonic loading and published in the literature.

4.1.1. Load–Deflection Response

The load–deflection relationships for seven control specimens are presented in Figure 18. The load–deflection response in Figure 18a,b compares the numerical and the experimental load–deflection response for beams CBA and FB30-1, respectively. Initially, the behavior of both specimens was linearly elastic, up to a load of approximately 20 kN for the FB30-1 specimen and 25 kN for the CBA specimen. Subsequently, the beams behave non-linearly until reaching a maximum load of 100 kN and 68 kN for FB30-1 and CBA specimens, respectively. This is followed by a yielding stage as an indication of flexural behavior for both specimens.

The load–deflection curves of the test specimens (C) and (N-1) are illustrated in Figure 18c,d, respectively. It can be stated that the actual response was satisfactorily captured by the developed finite element models. The comparison between the experimentally and numerically obtained results confirmed the reliability of the proposed finite element models in predicting the experimental outcomes. Although the specimens demonstrated a slight initial stiffness deviation, overestimation, or underestimation of the loading capacity and the deflection, they offered a good overall response such that both the experimental and the numerical patterns exhibited ductile behavior under monotonic loading. This has been observed through the acceptable degree of matching between the experimental and the numerical peak loads together with the corresponding deflections, the yielding loads, maximum deflections, and pre and post-cracking stiffness.

Figure 18e–g represent the load–deflection relationships of specimens that belong to three different categories. These categories differ in the arrangement of the transverse steel. S0 indicates non-transverse steel along the shear span specimen, S1 implies a specimen with steel stirrups at 175 mm intervals, whereas S3 means that the specimen owns steel stirrups spaced at every 260 mm. As can be depicted, the initial stiffness is accurately predicted by the finite element models for both specimens CON-S0 and CON-S1, while there is a slight overestimation for the CON-S3 specimen. This can be attributed to the fact that the numerical analysis usually considers the ideal status of the concrete material, which is perfect with no signs of damage or cracks. In reality, the concrete material is imperfect due to the presence of hairy cracks.

Table 5 summarizes the specimens' experimental and numerical ultimate and failure load-carrying capacities as well as their corresponding ultimate and failure deflection, respectively. Moreover, the mean numerical-to-experimental ultimate load carrying capacity is 3.15% with a standard deviation of 3.10, whereas the mean numerical-to-experimental ultimate load carrying capacity is 5.28% with a standard deviation of 5.10 for the failure load.

Table 5. Comparison between Numerical and Experimental Results of Control Specimens.

Number	Specimen	Experimental Results				Numerical Results				Difference (%) ¹			
		P_{ult} (kN)	δ_{ult} (mm)	P_f (kN)	δ_f (mm)	P_{ult} (kN)	δ_{ult} (mm)	P_f (kN)	δ_f (mm)	P_{ult} (%)	δ_{ult} (%)	P_f (%)	δ_f (%)
1	CBA [48]	77.95	14.23	71.04	26.34	78.17	6.86	75.38	13.29	0.28	0.53	6.11	49.54
2	C [49]	105.32	17.09	88.01	32.66	98.39	15.40	81.15	31.86	6.58	9.90	7.79	2.45
3	N-1 [50,51]	75.14	15.02	75.14	15.02	77.19	17.86	77.19	17.86	2.73	18.91	2.73	18.91
4	FB30-1 [7]	106.48	16.80	109.49	11.50	99.08	15.20	109.67	8.87	6.95	9.52	0.16	22.87
7	CON-S0 [52,53]	123.48	2.64	107.72	3.38	123.61	2.91	123.61	2.91	0.11	10.23	14.75	13.91
8	CON-S1 [52,53]	349.68	11.82	349.68	11.82	331.18	9.65	331.18	9.65	5.29	18.36	5.29	18.36

Table 5. Cont.

Number	Specimen	Experimental Results				Numerical Results				Difference (%) ¹			
		P_{ult} (kN)	δ_{ult} (mm)	P_f (kN)	δ_f (mm)	P_{ult} (kN)	δ_{ult} (mm)	P_f (kN)	δ_f (mm)	P_{ult} (%)	δ_{ult} (%)	P_f (%)	δ_f (%)
9	CON-S3 [52,53]	283.38	11.31	283.38	11.31	283.04	10.63	283.04	10.63	0.12	6.01	0.12	6.01
Mean									3.15	10.49	5.28	18.86	
Standard Deviation									3.10	6.50	5.10	15.37	

¹ Calculated as [(Numerical-Experimental)/(Experimental)] × 100.

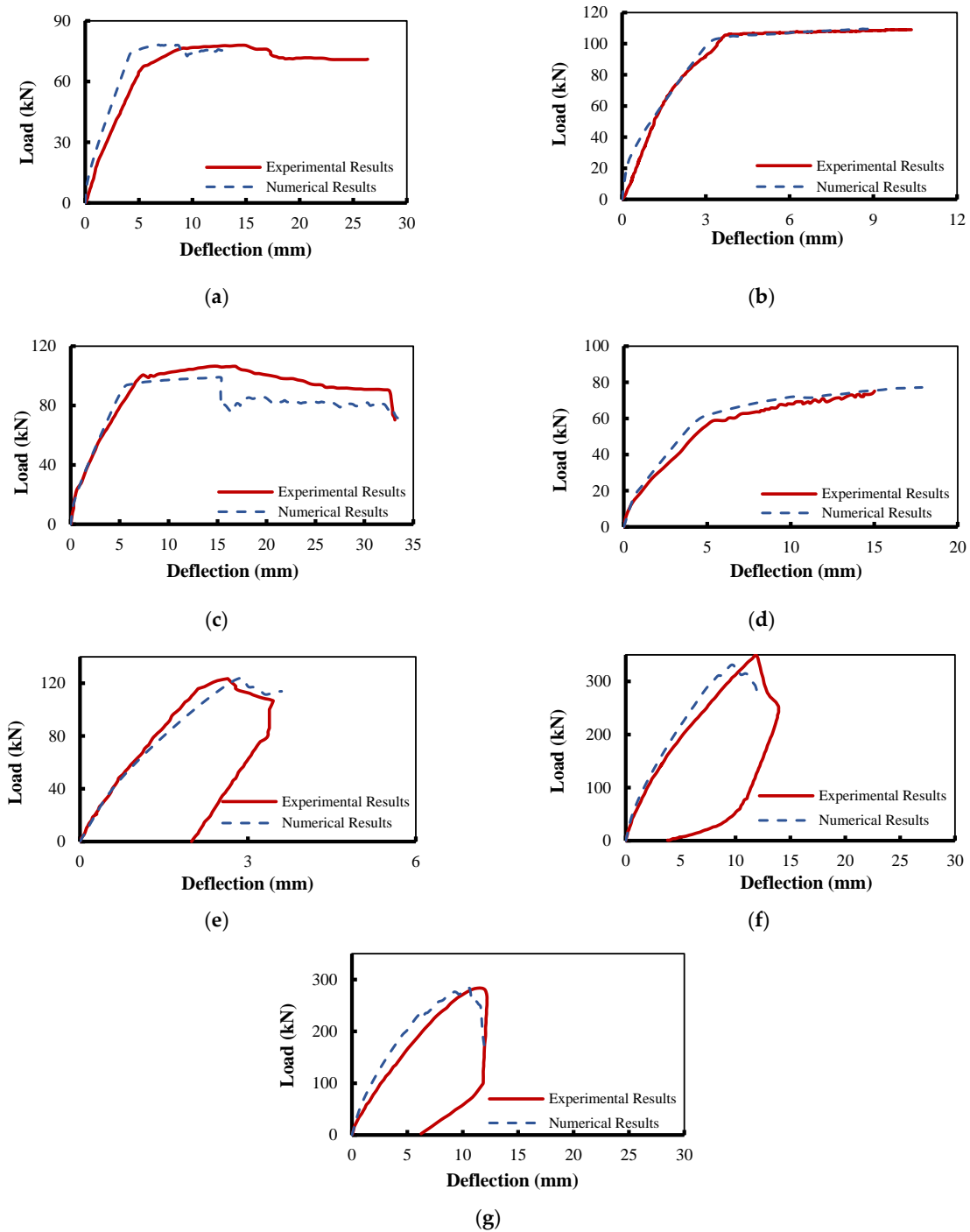


Figure 18. Load–Deflection Response: (a) Specimen (CBA); (b) Specimen (C); (c) Specimen (N-1); (d) Specimen (FB30-1); (e) Specimen (CON-S0); (f) Specimen (CON-S1); (g) Specimen (CON-S3).

4.1.2. Failure Mode and Crack Pattern

All three specimens tested by Chaallal et al. (CON-S0, SON-S1, CON-S3) failed due to the shear mode of failure [53,56] in the form of diagonal shear crack, which is confirmed by the numerical model. Figure 19 represents a typical failure mode obtained from the numerical model.

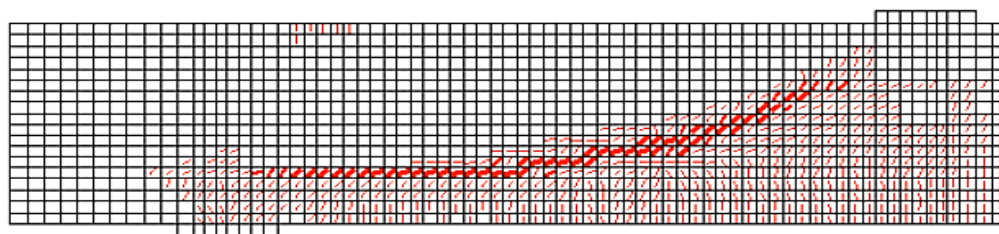


Figure 19. Mode of Failure of Specimens CON-S0, CON-S1, and CON-S3.

Figure 20a represents the experimental failure mode along with the crack width and the crack spacing of specimen CBA. This specimen experienced flexure failure mode, which was successfully detected by the numerical model. Figure 20b–e clarify the software’s capability to capture the stages of failure for a such specimen that begins with the crack initiation followed by propagation at different stages of failure.

Figure 21 illustrates the crack spacing (mm) of the same specimen at complete failure.

4.2. Validation of FRP Shear-Strengthened Specimens

The current numerical study involves the modification of some of the specimens previously modeled to accommodate the addition of FRP composites for shear-strengthening. The predictions of the finite element model are compared to the test results to validate the model’s accuracy. The FRP composites are simulated using two modeling approaches: smeared layer element and discrete truss element. Figure 22a–f illustrate the experimental and numerical load–deflection curves of the FRP shear-strengthened specimens.

4.2.1. Load–Deflection Response

Comparison between the numerical prediction and experimental results of specimens S1-0.33R and S3-EB reveals that both modeling approaches for FRP composites confirmed a good agreement with the experimental curves. However, the numerical results overestimate the load-carrying capacity of the FRP shear-strengthened specimens. In addition, the initial stiffness is slightly overestimated, as observed in Figure 22a,c. The degree of convergence between the experimentally recorded results and those obtained numerically is larger when adopting the discrete truss elements for FRP composites. This type of element provides approximately identical initial stiffness to the experimental behavior, as illustrated in Figure 22b,d. Using the smeared layer approach, the ultimate load-carrying capacity and the failure deflection are accurately predicted for the FB30-2 and FB30-3 specimens, as shown in Figure 22e–f.

Table 6 compares the smeared layer and discrete truss approaches in terms of ultimate strength and maximum deflection. The table indicates that the numerical models are affected by the simulation method of the FRP composites. Implementing the discrete truss element method to simulate the FRP composites showed accurate numerical predictions of FRP shear-strengthened beams under monotonic loading compared to the smeared layer method. The table indicates that the mean numerical-to-experimental ultimate load carrying capacity is 2.32% with a standard deviation of 3.10 when using smeared layer element, whereas the mean numerical-to-experimental ultimate load carrying capacity is 1.89% with a standard deviation of 1.24 for the discrete layer element. The importance of ductility in the structures has been investigated by many researchers. It is well documented in numerous publications that FRP shear-strengthened specimens fail at low ductility, which is called brittle failure [57,58].

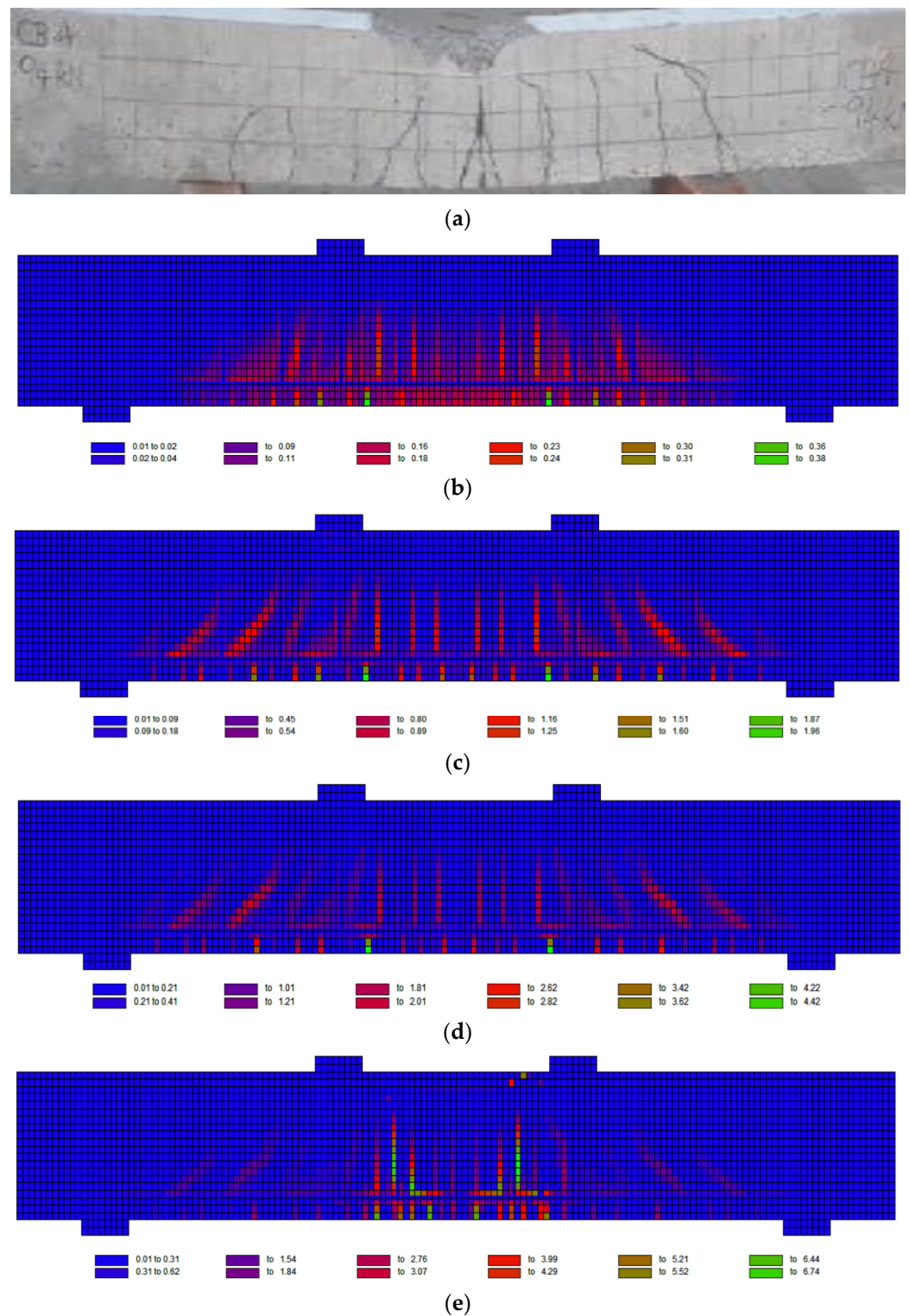


Figure 20. Crack Width (mm) and Failure Mode of Specimen (CBA): (a) Experimental failure mode [48]; (b) Cracking at 26% of the Ultimate Load; (c) Cracking at 65% of the Ultimate Load; (d) Cracking at 90% of the Ultimate Load; (e) Cracking at 100% of the Ultimate Load.

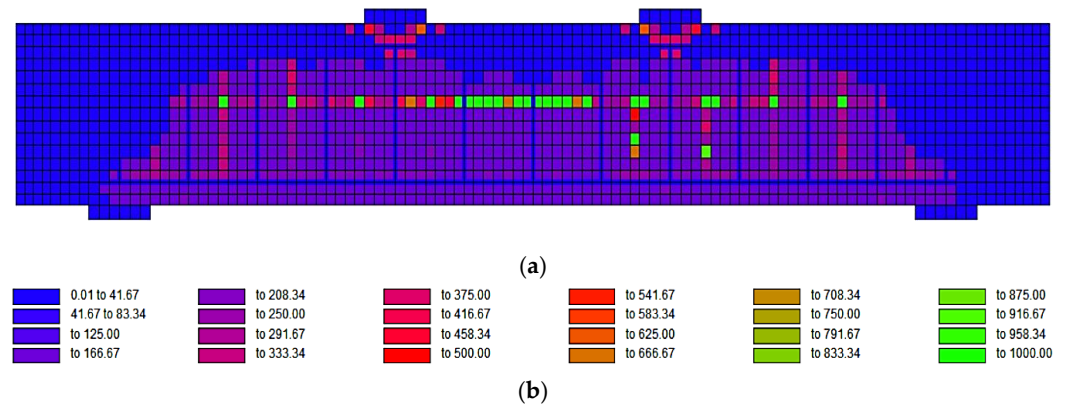


Figure 21. Crack Information of Specimen (CBA): (a) Crack Width and (b) Crack Spacing.

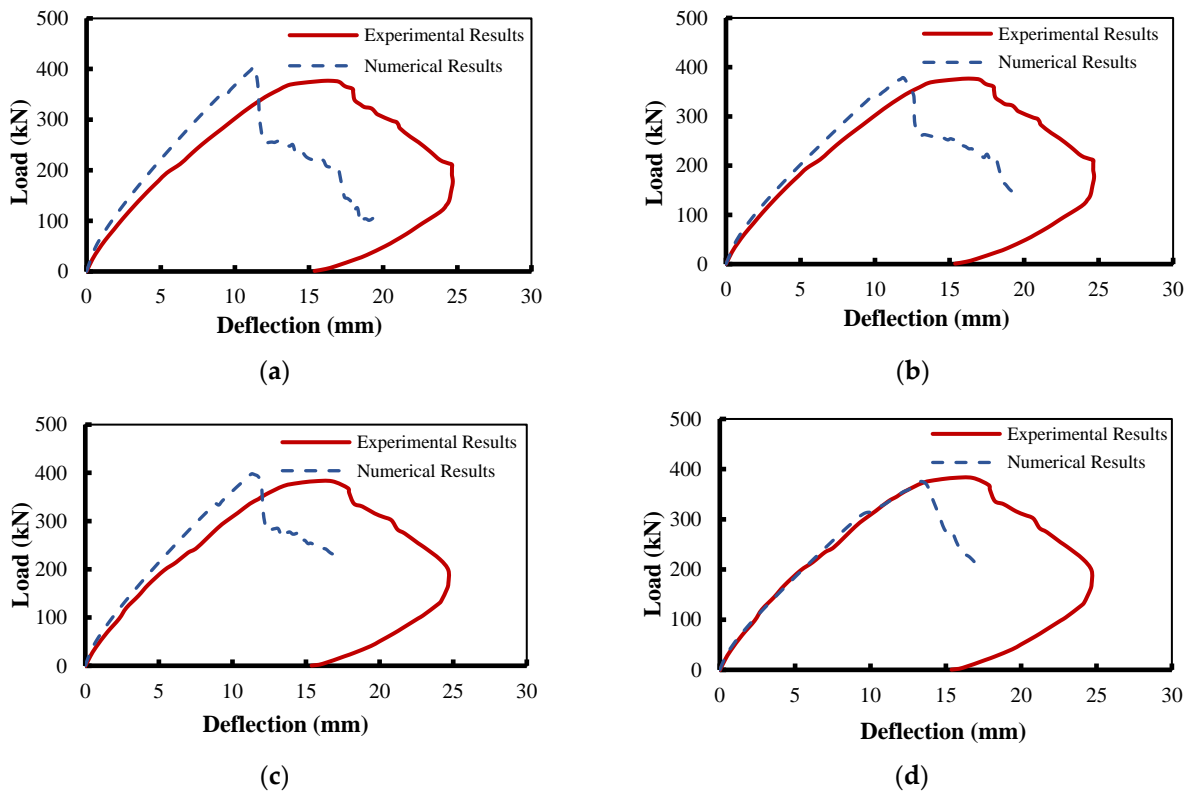


Figure 22. Cont.

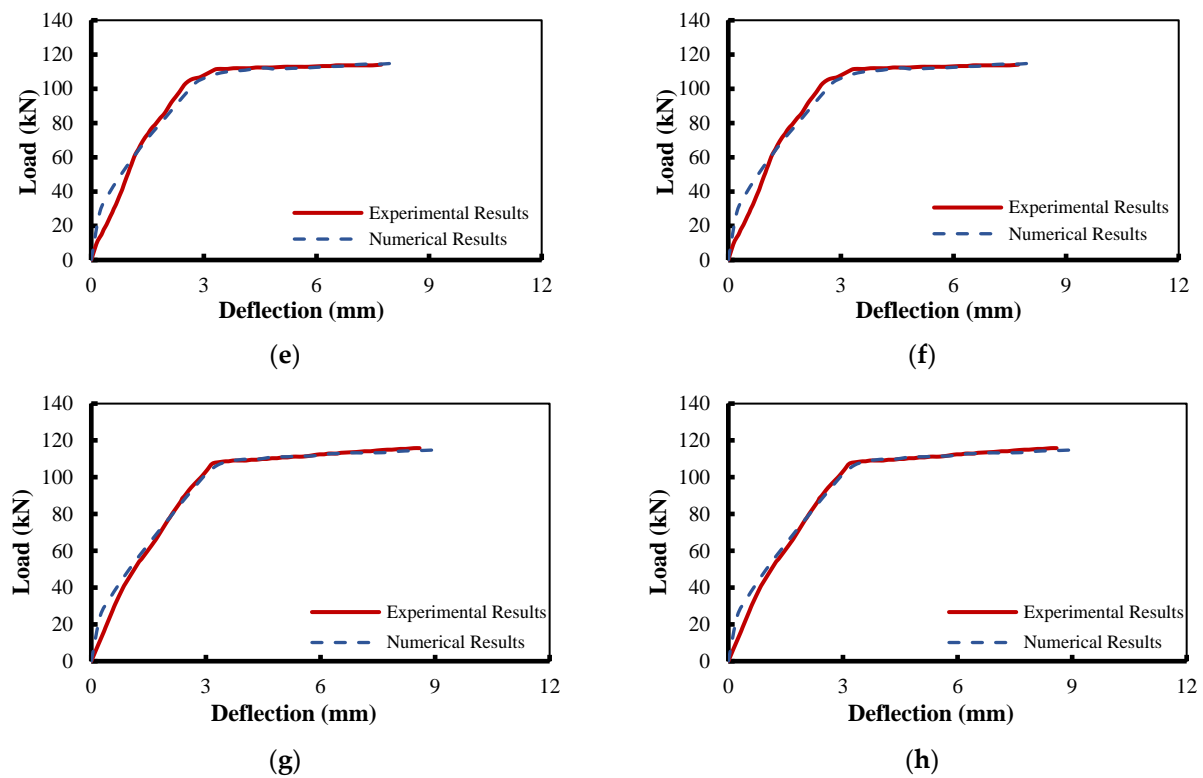


Figure 22. Load–Deflection Response: (a) S1-0.33R (FRP as Smearred Layer Element); (b) S1-0.33R (FRP as Discrete Truss Element); (c) S3-EB (FRP as Smearred Layer Element); (d) S3-EB (FRP as Discrete Truss Element); (e) FB30-2 (FRP as Smearred Layer Element); (f) FB30-2 (FRP as Discrete Truss Element); (g) FB30-3 (FRP as Smearred Layer Element); (h) FB30-3 (FRP as Discrete Truss Element).

Table 6. Comparison between Smearred Layer and Discrete Truss Elements to Model FRP Composites.

No.	Specimen	Experimental Results		Numerical Results				Difference (%)			
		P_{ult} (kN)	δ_{ult} (mm)	SL ¹		DT ²		SL		DT	
5	FB30-2 [7]	114.37	7.68	114.88	8.17	114.88	8.17	0.45	6.38	0.45	6.38
6	FB30-3 [7]	107.37	3.17	108.52	3.57	108.52	3.57	1.07	12.62	1.07	12.62
10	S1-0.33R [2,54–56]	376.63	16.53	403.62	11.29	367.74	12.16	7.17	31.70	2.36	26.44
11	S3-EB [2,54–56]	382.54	16.78	380.32	11.96	368.48	13.74	0.58	28.72	3.68	18.12
Mean								2.32	19.86	1.89	15.89
Standard Deviation								2.81	10.64	1.24	7.37

¹ Smearred layer element; ² discrete truss element.

4.2.2. Failure Mode and Crack Pattern

To fully account for the damage mechanism when FRP composites are considered, the failure modes have to be announced, discussed, and investigated. In this regard, the S3-EB specimen [53] failed due to the crushing of the concrete mode of failure, which is identical to the numerical failure mode. Figure 23 shows the crack pattern as obtained numerically.

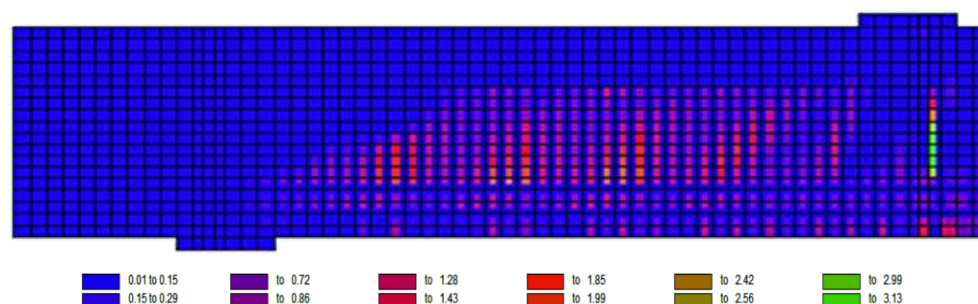


Figure 23. Numerical Crack Width (Pattern) and Failure Mode of Specimen (S3-EB).

The failure mode of the FB30-2 specimen that was tested by Dong et al. [7] is a flexural failure mode, which is comparable to the numerical one. Figure 24 illustrates the numerical crack pattern at failure, which confirms the efficiency of the non-linear finite element models.

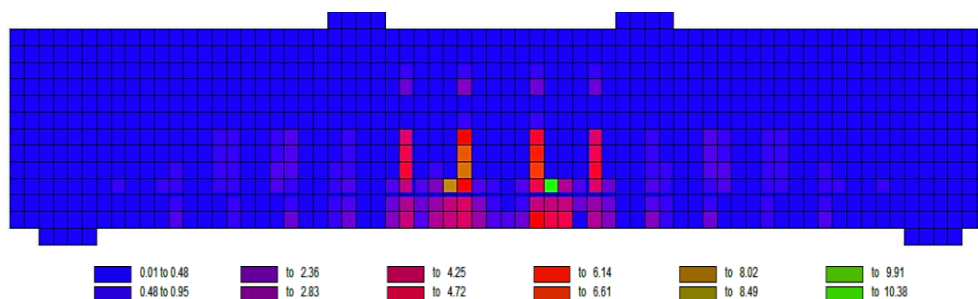


Figure 24. Numerical Crack Width (Pattern) and Failure Mode of Specimen (FB30-2).

5. Conclusions

Finite element models were developed using the VecTor2 software to address the behavior of FRP shear-strengthened beams. Appropriate non-linear constitutive models, as well as structural elements, were adopted to represent the behavior of concrete, reinforcing steel, loading plates, and FRP composites. The latter was simulated using two different modeling approaches: discrete truss and smeared layer elements. The best modeling approach for the FRP composites was selected on the basis of the accuracy of the numerical predictions compared to the experimental results. In this study, a total of seven control RC beams and four FRP shear-strengthened RC beams were analyzed to investigate the validity of the numerical model. The numerical predictions were compared with published experimental data in terms of ultimate loading capacities, load–deflection relations, crack patterns, and failure modes. Based on the results obtained, the following conclusions can be obtained:

- The numerical model results showed very good correlations when compared to experimental ones in terms of the ultimate carrying capacities and load–deflection relationships. This indicates that the VecTor2 finite element model software, which is developed based on the MCFT, is a successful candidate for simulating RC beams when loaded monotonically;
- The numerical models can notably provide an accurate simulation of the structural performance at the pre-peak behavior, post-peak behavior, failure mode, crack patterns, and maximum deflections;
- The two options for modeling the FRP composites indicate that both modeling options are effective for representing the behavior of FRP composites since, somehow, similar results were obtained;
- The concluded results reveal that the numerical models can successfully detect the crack propagation until failure;

- For FRP shear-strengthened beams, the predicted results showed that both methods adopted to simulate the FRP composites (discrete truss elements and Smeared layer element) compare very well to the experimental results.

This investigation studied the modeling of FRP shear-strengthened RC beams when implementing the MCFT. The developed numerical model in this study represents an initial step towards a reliable, valid, and robust model to simulate the performance of FRP shear-strengthened beams. Additional finite element models for another experimental test should be carried out with consideration of the FRP/concrete interfacial behavior.

Author Contributions: Conceptualization, N.I., S.E. and A.G.; methodology, N.I., S.E., A.G. and A.E.-K.; software, N.I. and S.E.; validation, N.I., S.E., A.G. and A.E.-K.; formal analysis, N.I., S.E., A.G. and A.E.-K.; investigation, N.I., S.E. and A.G.; resources, N.I., S.E. and A.G.; writing—original draft preparation, N.I., S.E. and A.G.; writing—review and editing, N.I., S.E., A.G. and A.E.-K.; visualization, N.I., S.E. and A.G.; supervision, S.E. and A.G.; project administration, A.G.; funding acquisition, A.G. All authors have read and agreed to the published version of the manuscript.

Funding: This research was funded by RESEARCH AFFAIRS OFFICE at the UNITED ARAB EMIRATES UNIVERSITY, grant number #31N375.

Institutional Review Board Statement: Not applicable.

Informed Consent Statement: Not applicable.

Data Availability Statement: All data, models, and code generated or used during the study appear in the submitted article.

Conflicts of Interest: The authors declare no conflict of interest. The funders had no role in the design of the study; in the collection, analyses, or interpretation of data; in the writing of the manuscript; or in the decision to publish the results.

References

1. Pohoryles, D.A.; Melo, J.; Rossetto, T. Combined Flexural and Shear Strengthening of RC T-Beams with FRP and TRM: Experimental Study and Parametric Finite Element Analyses. *Buildings* **2021**, *11*, 520. [\[CrossRef\]](#)
2. Chaallal, O.; Boussaha, F.; Bousselham, A. Fatigue Performance of RC Beams Strengthened in Shear with CFRP Fabrics. *J. Compos. Constr.* **2010**, *14*, 415–423. [\[CrossRef\]](#)
3. Naser, M.Z.; Hawileh, R.A.; Abdalla, J. Modeling Strategies of Finite Element Simulation of Reinforced Concrete Beams Strengthened with FRP: A Review. *J. Compos. Sci.* **2021**, *5*, 19. [\[CrossRef\]](#)
4. Sbahieh, S.; Rabie, M.; Ebead, U.; Al-Ghamdi, S.G. The Mechanical and Environmental Performance of Fiber-Reinforced Polymers in Concrete Structures: Opportunities, Challenges and Future Directions. *Buildings* **2022**, *12*, 1417. [\[CrossRef\]](#)
5. Rajak, D.K.; Pagar, D.D.; Menezes, P.L.; Linul, E. Fiber-Reinforced Polymer Composites: Manufacturing, Properties, and Applications. *Polymers* **2019**, *11*, 1667. [\[CrossRef\]](#) [\[PubMed\]](#)
6. Qureshi, J. A Review of Fibre Reinforced Polymer Structures. *Fibers* **2022**, *10*, 27. [\[CrossRef\]](#)
7. Dong, J.; Wang, Q.; Guan, Z. Structural behaviour of RC beams externally strengthened with FRP sheets under fatigue and monotonic loading. *Eng. Struct.* **2012**, *41*, 24–33. [\[CrossRef\]](#)
8. Teng, J.G.; Lam, L.; Chen, J.F. Shear strengthening of RC beams with FRP composites. *Prog. Struct. Eng. Mater.* **2004**, *6*, 173–184. [\[CrossRef\]](#)
9. Bank, L.C. *Composites for Construction: Structural Design with FRP Materials*; John Wiley & Sons: Hoboken, NJ, USA, 2006.
10. Teng, J.G.; Chen, J.F.; Smith, S.T. Debonding Failures in FRP-Strengthened RC Beams: Failure Modes, Existing Research and Future Challenges. In *Composites in Construction*; Wiley Online Library: Capri, Italy, 2001. [\[CrossRef\]](#)
11. *ACI 440.2R-08. 2008*; Guide for the Design and Construction of Externally Bonded FRP Systems for Strengthening Concrete Structures. ACI Committee 440: Farmington Hills, MI, USA, 2008.
12. Wong, P.S.; Vecchio, F.J.; Trommels, H. *Vector2 & Formworks User's Manual Second Edition*; University of Toronto: Toronto, ON, Canada, 2013.
13. Baingo, D. A Framework for Stochastic Finite Element Analysis of Reinforced Concrete Beams Affected by Reinforcement Corrosion. Ph.D. Thesis, University of Ottawa, Ottawa, ON, Canada, 2012. [\[CrossRef\]](#)
14. Godat, A.; Neale, K.W.; Labossière, P. Numerical Modeling of FRP Shear-Strengthened Reinforced Concrete Beams. *J. Compos. Constr.* **2007**, *11*, 640–649. [\[CrossRef\]](#)
15. Chen, G.; Chen, J.; Teng, J. On the finite element modelling of RC beams shear-strengthened with FRP. *Constr. Build. Mater.* **2012**, *32*, 13–26. [\[CrossRef\]](#)

16. Chen, G. Behaviour and Strength of RC Beams Shear-Strengthened with Externally Bonded FRP Reinforcement. 2010. Available online: <https://theses.lib.polyu.edu.hk/handle/200/5740> (accessed on 20 June 2022).
17. Arduini, M.; Nanni, A.; Di Tommaso, A.; Focacci, F. Shear response of continuous RC beams strengthened with carbon FRP sheets. In Proceedings of the Third International Symposium on Non-Metallic (FRP) Reinforcement on Concrete Structures, Sapporo, Japan, 14–16 October 1997.
18. Malek, A.; Saadatmanesh, H. Ultimate Shear Capacity of Reinforced Concrete Beams Strengthened with Web-Bonded Fiber-Reinforced Plastic Plates. *ACI Struct. J.* **1998**, *95*, 391–399. [[CrossRef](#)]
19. Malek, A.; Saadatmanesh, H. Analytical Study of Reinforced Concrete Beams Strengthened with Web-Bonded Fiber Reinforced Plastic Plates or Fabrics. *ACI Struct. J.* **1998**, *95*, 343–352. [[CrossRef](#)]
20. Kachlakev, D.; McCurry, D. Behavior of full-scale reinforced concrete beams retrofitted for shear and flexural with FRP laminates. *Compos. Part B Eng.* **2000**, *31*, 445–452. [[CrossRef](#)]
21. Wong, R. Towards Modelling of Reinforced Concrete Members with Externally-Bonded Fibre Reinforced Polymer, FRP, Composites. Master's Thesis, University of Toronto, Toronto, ON, Canada, 2001. Available online: <https://library-archives.canada.ca/eng/services/services-libraries/theses/Pages/item.aspx?idNumber=1006758496> (accessed on 24 February 2023).
22. Vecchio, F.J.; Collins, M.P. The modified compression-field theory for reinforced concrete elements subjected to shear. *ACI J.* **1986**, *83*, 219–231.
23. Salgado, R.A.; Guner, S. A Numerical Analysis Methodology for the Strengthening of Deep Cap Beams. *Spec. Publ.* **2019**, *333*, 1–18. [[CrossRef](#)]
24. Benmokrane; Neale, K.W.; Belarbi, A.; Yahia, A. Performance and Strut Efficiency Factor of Concrete Deep Beams Reinforced With Gfrp Bars. Ph.D. Thesis, University of Sherbrooke, Sherbrooke, QC, Canada, 2015.
25. Rezvanisharif, M.; Ketabi, M.S. FE Modeling and Seismic Performance Evaluation of Hybrid SMA-Steel RC Beam-Column Joints. *Lat. Am. J. Solids Struct.* **2019**, *16*, e192. [[CrossRef](#)]
26. Habibi, S. Finite Element Modelling of Corrosion Damaged Reinforced Concrete Structures. Master's Thesis, University of Toronto, Toronto, ON, Canada, 2017. Available online: <https://www.proquest.com/docview/1934400235?pq-origsite=gscholar&fromopenview=true> (accessed on 1 February 2023).
27. Bentz, E.C.; Vecchio, F.J.; Collins, M.P. Simplified Modified Compression Field Theory for Calculating Shear Strength of Reinforced Concrete Elements. *ACI Struct. J.* **2006**, *103*, 614–624. [[CrossRef](#)]
28. Vass, G. Finite Element Modelling of Different Strengthening Strategies for Reinforced Concrete Deep Beams. Master's Thesis, Université de Liège, Liège, Belgique, 2018. Available online: <https://matheo.uliege.be/handle/2268.2/4439> (accessed on 27 February 2022).
29. Sadeghian, V.; Vecchio, F. The Modified Compression Field Theory: Then and Now. *ACI Struct. J.* **2018**, *328*, 20. [[CrossRef](#)]
30. Comparison of Nonlinear Finite Element Modeling Tools for Structural Concrete. Available online: https://scholar.google.com/scholar?hl=en&as_sdt=0%2C5&q=Comparison+of+Nonlinear+Finite+Element+Modeling+Tools+for+Structural+Concrete&btnG= (accessed on 2 December 2022).
31. Ceresa, P.; Viquez, A.G. Nonlinear Analysis of Shear Critical Rc Members Using Current Fe Software. In Proceedings of the 6th International Conference on Computational Methods in Structural Dynamics and Earthquake Engineering Methods in Structural Dynamics and Earthquake Engineering, Rhodes Island, Greece, 15–17 June 2017. [[CrossRef](#)]
32. Arafa, A.; Farghaly, A.S.; Benmokrane, B. Nonlinear Finite-Element Analysis for Predicting the Behavior of Concrete Squat Walls Reinforced with GFRP Bars. *J. Struct. Eng.* **2019**, *145*, 04019107. [[CrossRef](#)]
33. Pathak, P.; Zhang, Y.X. Finite Element Simulation for Nonlinear Finite Element Analysis of FRP Strengthened RC Beams with Bond-Slip Effect. *Appl. Mech. Mater.* **2016**, *846*, 440–445. [[CrossRef](#)]
34. Rasheed, H.A. *Strengthening Design of Reinforced Concrete with FRP*; CRC Press: Boca Raton, FL, USA, 2014. [[CrossRef](#)]
35. Arafa, A.; Ahmed, N.; Farghaly, A.S.; Chaallal, O.; Benmokrane, B. Exploratory Study on Incorporating Glass FRP Reinforcement to Control Damage in Steel-Reinforced Concrete Bridge Pier Walls. *J. Bridg. Eng.* **2021**, *26*, 04020116. [[CrossRef](#)]
36. Al-Rousan, R.; Issa, M. Fatigue performance of reinforced concrete beams strengthened with CFRP sheets. *Constr. Build. Mater.* **2011**, *25*, 3520–3529. [[CrossRef](#)]
37. Kent, D.C.; Park, R. Flexural Members with Confined Concrete. *J. Struct. Div.* **1971**, *97*, 1969–1990. [[CrossRef](#)]
38. Junior, S.A.A.; Parvin, A. Performance of Continuous Concrete Beams with Reinforced FRP Bars and Sheets. In Proceedings of the 5th International Conference on Smart Monitoring, Assessment and Rehabilitation of Civil Structures, Potsdam, Germany, 27–29 August 2019; p. 8.
39. Baji, H.; Eslami, A.; Ronagh, H. Development of a nonlinear FE modelling approach for FRP-strengthened RC beam-column connections. *Structures* **2015**, *3*, 272–281. [[CrossRef](#)]
40. Ibrahim, N.; Elkholly, S.; Godat, A. Finite Element Simulation of Reinforced Concrete Beams under Fatigue Loading. In Proceedings of the 7th World Congress on Civil, Structural, and Environmental Engineering, CSEE 2022, Lisbon, Portugal, 10–12 April 2022. [[CrossRef](#)]
41. Ibrahim, A.M.; Mahmood, M.S. Finite Element Modeling of Reinforced Concrete Beams Strengthened with FRP Laminates. *Eur. J. Sci. Res.* **2009**, *30*, 526–541.
42. Godat, A.; Labossière, P.; Neale, K.W.; Chaallal, O. Behavior of RC members strengthened in shear with EB FRP: Assessment of models and FE simulation approaches. *Comput. Struct.* **2012**, *92–93*, 269–282. [[CrossRef](#)]

43. Ferreira, D.; Oller, E.; Marí, A.; Bairán, J. Numerical Analysis of Shear Critical RC Beams Strengthened in Shear with FRP Sheets. *J. Compos. Constr.* **2013**, *17*, 04013016. [[CrossRef](#)]
44. Prajapati, G.N.; Aalok, A.D.P.; Reddy, T.B. Finite Element Simulation of Shear Strengthened Rc Beams Externally Reinforced with Frp. 2021, Volume 18, No. 3, pp. 357–370, January 2017. Available online: <https://www.sid.ir/en/Journal/ViewPaper.aspx?ID=517766> (accessed on 26 December 2021).
45. Said, S.; Sadeghian, V.; Lau, D. Modelling of Frp-Strengthened Shear Walls With Special Consid-Eration to End-Anchorage and Debonding Effects. In Proceedings of the 17th World Conference on Earthquake Engineering, Sendai, Japan, 13–18 September 2020; p. 13.
46. Palermo, D.; Vecchio, F.J. Simulation of Cyclically Loaded Concrete Structures Based on the Finite-Element Method. *J. Struct. Eng.* **2007**, *133*, 728–738. [[CrossRef](#)]
47. Shin, D.-H.; Kim, H.-J. Cyclic response of rectangular RC columns retrofitted by hybrid FRP sheets. *Structures* **2020**, *28*, 697–712. [[CrossRef](#)]
48. Murthy, A.R.; Karihaloo, B.; Rani, P.V.; Priya, D.S. Fatigue behaviour of damaged RC beams strengthened with ultra high performance fibre reinforced concrete. *Int. J. Fatigue* **2018**, *116*, 659–668. [[CrossRef](#)]
49. Banjara, N.K.; Ramanjaneyulu, K. Investigations on behaviour of flexural deficient and CFRP strengthened reinforced concrete beams under static and fatigue loading. *Constr. Build. Mater.* **2019**, *201*, 746–762. [[CrossRef](#)]
50. Papakonstantinou, C.G.; Petrou, M.F.; Harries, K.A. Fatigue Behavior of RC Beams Strengthened with GFRP Sheets. *J. Compos. Constr.* **2001**, *5*, 246–253. [[CrossRef](#)]
51. Papakonstantinou, G.; Balaguru, P.N.; Petrou, M.F. *Analysis of Reinforced Concrete Beams Strengthened with Composites Subjected to Fatigue Loading*; ACI Special Publication: Farmington Hills, MI, USA, 2002; pp. 41–60.
52. Mofidi, A.; Chaallal, O. Shear Strengthening of RC Beams with Externally Bonded FRP Composites: Effect of Strip-Width-to-Strip-Spacing Ratio. *J. Compos. Constr.* **2011**, *15*, 732–742. [[CrossRef](#)]
53. Bourget, S.; El-Saikaly, G.; Chaallal, O. Behavior of Reinforced Concrete T-Beams Strengthened in Shear Using Closed Carbon Fiber-Reinforced Polymer Stirrups Made of Laminates and Ropes. *ACI Struct. J.* **2017**, *114*, 1087–1098. [[CrossRef](#)]
54. El-Saikaly, G.; Chaallal, O. Extending the Fatigue Life of Reinforced Concrete T-Beams Strengthened in Shear with Externally Bonded FRP: Upgrading versus Repairing. *J. Compos. Constr.* **2015**, *19*, 04014027. [[CrossRef](#)]
55. El-Saikaly, G.; Chaallal, O. Fatigue behavior of RC T-beams strengthened in shear with EB CFRP L-shaped laminates. *Compos. Part B Eng.* **2015**, *68*, 100–112. [[CrossRef](#)]
56. Mofidi, A.; Thivierge, S.; Chaallal, O.; Shao, Y. Behavior of Reinforced Concrete Beams Strengthened in Shear Using L-Shaped CFRP Plates: Experimental Investigation. *J. Compos. Constr.* **2014**, *18*, 04013033. [[CrossRef](#)]
57. Gusella, F. Effect of the plastic rotation randomness on the moment redistribution in reinforced concrete structures. *Eng. Struct.* **2021**, *252*, 113652. [[CrossRef](#)]
58. D’Angela, D.; Magliulo, G.; Celano, F.; Cosenza, E. Characterization of local and global capacity criteria for collapse assessment of code-conforming RC buildings. *Bull. Earthq. Eng.* **2021**, *19*, 3701–3743. [[CrossRef](#)]

Disclaimer/Publisher’s Note: The statements, opinions and data contained in all publications are solely those of the individual author(s) and contributor(s) and not of MDPI and/or the editor(s). MDPI and/or the editor(s) disclaim responsibility for any injury to people or property resulting from any ideas, methods, instructions or products referred to in the content.